DRAFT VERSION NOVEMBER 16, 2010
Preprint typeset using LaTeX style emulateapj v. 11/10/09

STATISTICS OF SATELLITE GALAXIES AROUND MILKY WAY-LIKE HOSTS

MICHAEL T. BUSHA[1,2], RISA H. WECHSLER[1,3], PETER S. BEHROOZI[1,3], BRIAN F. GERKE[1,3], ANATOLY KLYPIN[4], AND JOEL PRIMACK[5]

Draft version November 16, 2010

ABSTRACT

We characterize the distribution of bright satellite galaxies like the Magellanic Clouds around Milky Way-like hosts using the high resolution cosmological N-body simulation Bolshoi. Our measurements indicate that, for Milky Way luminosity hosts, there is just a 5% chance of hosting two satellites with similar properties as the Magellanic Clouds inside the virial radius of the host halo. Under the assumption of a tight relationship between galaxy luminosities and halo velocities, we make detailed comparisons to similar measurements using SDSS DR7 data by Liu et al. (2010). Excellent agreement is found for models selected by kinematic properties ($v_{\rm max}$) as well as by luminosity: models and data predict very similar probabilities for having zero, one, and two systems, and find that the likelihood of a system like the MW and MCs is rare. In addition, we present a prediction for the probability for a host galaxy to have N_{subs} satellite galaxies brighter than a given luminosity, as a function of the magnitudes of both the host and satellite. This probability and its scaling with host properties is significantly different than that of mass-selected objects because of scatter in the mass-luminosity relation and because of variations in the star formation efficiency with halo mass.

Subject headings: galaxies: dwarf, Magellanic Clouds, evolution — dark matter

1. INTRODUCTION

Understanding the satellite population of our own Milky Way galaxy is one of the outstanding problems in galaxy evolution studies today. Because these objects have weak gravitational potential wells, it is quite likely that different physical processes will play a driving role in determining how such galaxies form and evolve than for brighter, more massive objects. One manifestation of this is the well-known "missing satellites problem", which refers to the fact that the number of satellite galaxies predicted from simulations appears to be much higher than the number actually observed around the Milky Way (Moore et al. 1999; Klypin et al. 1999). One common way to address this problem has been to run simulations of individual objects using extremely high mass resolution. To date, roughly 10 of these ultra-high resolution N-body simulations have been run, which typically resolve individual Milky Way mass halos with upwards of 10^9 particles (Madau et al. 2008; Springel et al. 2008; Stadel et al. 2009).

While not a part of the missing satellite problem, one common feature of these ultra-high resolution simulations is that typically under predict the number of massive satellites compared to those in our Milky Way (see, e.g., Figure 5 in Madau et al. 2008). Indeed, most of these high resolution halos contain no objects of similar mass to the Magellanic Clouds, of which the Milky Way has two. While this should hardly be taken as a serious problem since the handful of high resolution simulated halos hardly constitute a statistical sample, understanding how typical or atypical the Milky Way is, and whether or not there is some sort of "extra satellites" problem at high masses, is important.

The Magellanic Clouds (MCs) are a pair of well studied systems in the Southern Hemisphere. While their large angular size makes detailed mass measurements somewhat difficult, recent observations constrain their maximum circular velocities to be around $v_{\rm max} \sim 60 {\rm km\ s^{-1}}$ (van der Marel et al. 2002; Stanimirović et al. 2004). However, because they are relatively nearby and have been studied with high-precision instruments such as HST for some time, detailed 3-dimensional measurements of their velocities have been made (Kallivayalil et al. 2006b,a). Some of these studies have indicated that the Magellanic Clouds may be on their first obit around the Milky Way (Besla et al. 2007; Busha et al. 2010), which may make such an extra satellite problem less worrisome, if the presence of the Magellanic Clouds is a transient event. Regardless of the dynamical state of the Magellanic clouds, it is an important test of galaxy formation to understand the likelihood for Milky Way like systems to host massive satellite galaxies.

Recent developments have afforded us the possibility to address this problem in more detail with both observations and theoretical models. From the observational side, wide area surveys such as the Sloan Digital Sky Survey (SDSS York et al. 2000; Abazajian et al. 2009) have given us the ability to probe galaxy content for a large number of Milky Way magnitude objects (Chen et al. 2006; James & Ivory 2010; Liu et al. 2010).

There has similarly been a significant amount of work on this field coming from the simulation side of things, which have found a wide range of results. Koposov et al. (2009) used a number of toy models to add galaxy properties to dark matter halos generated using a combination of Press-Schechter theory with semi-analytic models for tracking subhalo orbit (i.e., Zentner et al. 2005). Here, they found it was very difficult to model objects as bright as Magellanic clouds without allowing for an extremely high star formation efficiency. Similarly, (Okamoto et al. 2010) explored a range of feedback

[1] Kavli Institute for Particle Astrophysics and Cosmology, Department of Physics, Stanford University, Stanford, CA, 94305 mbusha@slac.stanford.edu, rwechsler@stanford.edu
[2] Institute for Theoretical Physics, University of Zurich, 8057 Zurich, Switzerland
[3] SLAC National Accelerator Laboratory, Menlo Park, CA, 94025, USA
[4] Astronomy Department, New Mexico State University, Las Cruces, NM, 88003
[5] Department of Physics, University of California, Santa Cruz, CA 95064, USA

Milky Way mass halos and counting the number of objects internal to their virial radii. We take the virial mass of the Milky Way to be $1.2 \times 10^{12} M_\odot$, **((need to give bin))** the mass measured in Busha et al. (2010) and consistent with most results in the literature (Battaglia et al. 2005; Dehnen et al. 2006; Smith et al. 2007; Xue et al. 2008). This leaves us with 48,000 Milky Way analogs in the Bolshoi volume. We present the result of this measurement as the colored points in the left panel of Figure 1. Here, the different colors represent different thresholds for satellite $v_{\rm max}$: red, green, and blue represent all satellites with $v_{\rm max} > 50$, 60, and 70 km s^{-1}. Error bars were calculated using the bootstrap method and show the 95% range. From this plot, we can immediately see that the likelihood of hosting multiple satellites is somewhat low. For satellites bigger than 50 km s^{-1}, roughly 30% of simulated hosts contain one or more subhalos and just 8% have two or more. These numbers are in excellent agreement with the work of Boylan-Kolchin et al. (2010) who performed a similar analysis on the Millennium II simulation, which was run using a different N-body code in a slightly different cosmology and with a very different subhalo identification algorithm. The probabilities drop significantly as we increase the mass of the subhalo, i.e. the probability of two subhalos bigger than $v_{\rm max} = 70$km s^{-1} is just 1%.

Upon initial inspection, these numbers appear somewhat low, with the existence of two satellites larger than 50km s^{-1} making the Milky Way almost a 2σ outlier. This motivates further investigation into what other properties correlate with satellite abundance. In particular, we investigate the correlation of the number of subhalos with host mass, concentration, and environment.

3.1. *Mass dependencies*

The correlation between subhalo abundance and host mass has been well studied (Zentner & Bullock 2003; Diemand et al. 2004; Gao et al. 2004; Zentner et al. 2005; Klypin et al. 2010). These studies have all found that, when scaled in units of $\mu = M_{sub}/M_{host}$, larger halos contain more subhalos above a given μ than do smaller ones. This is the expected result from the hierarchical merging picture of CDM, where larger objects grow through the merging of smaller objects and therefore form later (Blumenthal et al. 1984; Lacey & Cole 1993). This later formation has a two-fold impact: it reduces the amount of time available to tidally strip a subhalo, and lowers the host concentration, further reducing the ability of a host to tidally strip its subhalos (Wechsler et al. 2002; Busha et al. 2007). Motivated by this, we present the abundance of LMC and SMC-mass subhalos for the 27,000 Bolshoi halos with $M_{\rm vir} \sim 2.6 \times 10^{12} M_\odot$. The results can be seen in Figure 1. Here, the left panel shows the results for selecting hosts with $M_{\rm vir} = 0.8 - 1.7 \times 10^{12} h^{-1} M_\odot$, while the right panel shows a mass range $M_{\rm vir} = 1.7 - 3.4 \times 10^{12} h^{-1} M_\odot$.

The cumulative probabilities for hosting two or more 50 km s^{-1}halos increases by a factor of 3 from the case of the $\sim 1 \times 10^{12}$ objects **(shouldn't this be 1.2 times?)** , increasing from 8% to 26%, while jumping by a factor of 6 to go from 1% to nearly 6% for 70km s^{-1}subhalos. We emphasize that this is not in fact a contradiction with the results of Busha et al. (2010), which found that a halo with exactly MC-like subhalos was likely to have mass $1.2 \times 10^{12} M_\odot$. While the fraction of 2.6×10^{12} halos hosting two large subhalos is larger, the slope of the mass function tells us that there are many more lower-mass, $1.2 \times 10^{12} M_\odot$ halos. Additionally, aside from just considering $v_{\rm max}$, Busha et al. (2010) weighted objects to look like the MCs in terms of location and three-dimensional velocity, properties not considered in the present analysis.

Again, these results are in excellent agreement with the work of Boylan-Kolchin et al. (2010). While such an agreement is generally expected from pure collisionless N-body simulations, such agreement is not as trivially expected as it may appear. While the present work uses results from the Bolshoi simulation, run using the adaptive refinement ART code and the BDM halo finder, Boylan-Kolchin et al. (2010) used the Millennium-II simulation run on the TreePM code Gadget-2 with substructures identified using the Subfind algorithm (Springel et al. 2001). Additionally, in both cases, we are concerned with subhalos close to the mass-limit for the simulation. Thus, the close agreement between these two works is a strong endorsement that numerical effects in the simulations are well-understood at this level.

3.2. *Environmental effects*

Beyond simple measurements of the mass dependence, the size of the cosmological volume modeled by the Bolshoi simulation allows us to perform further detailed studies on properties impacting this distribution. Here, we quantify the environmental dependence of the subhalo population by splitting the sample on a local density, defined by

$$\delta_{h,r} = \frac{\rho_{h,r} - \bar{\rho}_h}{\bar{\rho}_h} \qquad (2)$$

where $\rho_{h,r}$ is the Eulerian density of dark matter contained in halos larger than $M_{\rm vir} = 2 \times 10^{11} M_\odot$ (roughly 1000 particles in Bolshoi) defined in a sphere of size r. We compare the distribution $P(N_{sats})$ for halos in the top and bottom quartile distributions with the mean relation in Figure 2. There is a clear systematic trend: halos living in overdense regions (blue points) are more likely to host massive subhalos than those in underdense regions (red points). This is likely due to the fact that halos in denser environments live in more biased regions, where smaller density perturbations are amplified, making it easier for smaller halos to form and accrete onto intermediate mass hosts. This makes the deviations from the mean relation in Figure 2 a potentially observable manifestation of assembly bias, which posits that the properties of a given halo may be determined by properties other than mass, such as the halo environment. Here, we measure densities on a scale of $1.0 h^{-1}$Mpc. We have performed a similar analysis on a range of scales and find this to be the range where the distribution is the most sensitive.

Selecting for objects in a dense environment increases the probability of having $N_{subs} = 2$ or more increases by almost 25%, from 9% to just over 11%. The effect gets stronger for hosts with larger values of N_{subs}. The Milky Way is somewhat overdense on this scale, having a massive companion M31 and a number of dwarf galaxies with total mass of roughly $(3-4) \times 10^{12} h^{-1} M_\odot$ (once the mass of the Milky Way itself is excluded Li et al. 2009). Even if all neighboring objects other than M31 are excluded, this puts the Milky Way in the top quartile of our measured mass distribution in Bolshoi. We can understand this by making an explicit cut for halos having nearby neighbors with $M_{\rm vir} = (1-3) \times 10^{12} M_\odot$ (green points), which boosts the $N_{subs} = 2$ probability by roughly 2-σ. Thus, the presence of M31 boosts the chance of seeing the Magellanic Clouds in the Milky Way.

of the Milky Way to be $\log(M_{\rm vir}/1{\rm M}_\odot) = 12.08 \pm 0.12$ ($M_{\rm vir} = 1.2 \times 10^{12}{\rm M}_\odot$), the mass measured in Busha et al. (2010) and consistent with most results in the literature (Battaglia et al. 2005; Dehnen et al. 2006; Smith et al. 2007; Xue et al. 2008). This leaves us with 36,000 Milky Way analogs in the Bolshoi volume. We present the result of this measurement as the colored points in the left panel of Figure 1. Here, the different colors represent different thresholds for satellite $v_{\rm max}$: red, green, and blue represent all satellites with $v_{\rm max} > 50$, 60, and 70 km s^{-1}. Error bars were calculated using the bootstrap method and show the 95% range. From this plot, we can immediately see that the likelihood of hosting multiple satellites is somewhat low. For satellites bigger than 50 km s^{-1}, roughly 30% of simulated hosts contain one or more subhalos and just 8% have two or more. These numbers are in excellent agreement with the work of Boylan-Kolchin et al. (2010) who performed a similar analysis on the Millennium II simulation, which was run using a different N-body code in a slightly different cosmology and with a very different subhalo identification algorithm. The probabilities drop significantly as we increase the mass of the subhalo, i.e., the probability of two subhalos bigger than $v_{\rm max} = 70$km s^{-1}is just 1%.

Upon initial inspection, these numbers appear somewhat low, with the existence of two satellites larger than 50km s^{-1} making the MW almost a 2σ outlier. Understanding if anything other than random chance is responsible for putting the MW in this slightly rare regime motivates further investigation into what other properties correlate with satellite abundance. In particular, we investigate the correlation of the number of subhalos with host mass and environment.

3.1. *Mass dependencies*

The correlation between subhalo abundance and host mass has been well studied (Zentner & Bullock 2003; Diemand et al. 2004; Gao et al. 2004; Zentner et al. 2005; Klypin et al. 2010). These studies have all found that, when scaled in units of $\mu = M_{sub}/M_{host}$, larger halos contain more subhalos above a given μ than do smaller ones. This is the expected result from the hierarchical merging picture of CDM, where larger objects grow through the merging of smaller objects and therefore form later (Blumenthal et al. 1984; Lacey & Cole 1993). This later formation has a two-fold impact: it reduces the amount of time available to tidally strip a subhalo, and lowers the host concentration, further reducing the ability of a host to tidally strip its subhalos (Wechsler et al. 2002; Busha et al. 2007). Motivated by this, we present the abundance of LMC and SMC-mass subhalos for the 27,000 Bolshoi halos with $M_{\rm vir} \sim 2.6 \times 10^{12}{\rm M}_\odot$. The results can be seen in Figure 1. Here, the left panel shows the results for selecting hosts with $M_{\rm vir} = 0.8 - 1.7 \times 10^{12}h^{-1}{\rm M}_\odot$, while the right panel shows a mass range $M_{\rm vir} = 1.7 - 3.4 \times 10^{12}h^{-1}{\rm M}_\odot$.

The cumulative probabilities for hosting two or more 50 km s^{-1}halos increases by a factor of 3 from the case of the 1.2×10^{12} objects , increasing from 8% to 26%, while jumping by a factor of 6 to go from 1% to nearly 6% for 70km s^{-1}subhalos. We emphasize that this is not in fact a contradiction with the results of Busha et al. (2010), which found that a halo with exactly MC-like subhalos was likely to have mass $1.2 \times 10^{12}{\rm M}_\odot$. While the fraction of 2.6×10^{12} halos hosting two large subhalos is larger, the slope of the mass function tells us that there are many more lower-mass, $1.2 \times 10^{12}{\rm M}_\odot$ halos. Additionally, aside from just considering $v_{\rm max}$, Busha et al. (2010) weighted objects to look like the MCs in terms of location and three-dimensional velocity, properties not considered in the present analysis.

Again, these results are in excellent agreement with the work of Boylan-Kolchin et al. (2010). While such an agreement is generally expected from pure collisionless N-body simulations, such agreement is not as trivially expected as it may appear. While the present work uses results from the Bolshoi simulation, run using the adaptive refinement ART code and the BDM halo finder, Boylan-Kolchin et al. (2010) used the Millennium-II simulation run on the TreePM code Gadget-2 with substructures identified using the Subfind algorithm (Springel et al. 2001). Additionally, in both cases, we are concerned with subhalos close to the mass-limit for the simulation. Thus, the close agreement between these two works is a strong endorsement that numerical effects in the simulations are well-understood at this level.

3.2. *Environmental effects*

Beyond simple measurements of the mass dependence, the size of the cosmological volume modeled by the Bolshoi simulation allows us to perform further detailed studies on properties impacting this distribution. Here, we quantify the environmental dependence of the subhalo population by splitting the sample on on a local density, defined by

$$\delta_{h,r} = \frac{\rho_{h,r} - \bar{\rho}_h}{\bar{\rho}_h} \qquad (2)$$

where $\rho_{h,r}$ is the Eulerian density of dark matter contained in halos larger than $M_{\rm vir} = 2 \times 10^{11}{\rm M}_\odot$ (roughly 1000 particles in Bolshoi) defined in a sphere of size r. We compare the distribution $P(N_{sats})$ for halos in the top and bottom quartile distributions with the mean relation in Figure 2. There is a clear systematic trend: halos living in overdense regions (blue points) are more likely to host massive subhalos than those in underdense regions (red points). This is likely due to the fact that halos in denser environments live in more biased regions, where smaller density perturbations are amplified, making it easier for smaller halos to form and accrete onto intermediate mass hosts. This makes the deviations from the mean relation in Figure 2 a potentially observable manifestation of assembly bias, which posits that the properties of a given halo may be determined by properties other than mass, such as the halo environment. Here, we measure densities on a scale of $1.0h^{-1}$Mpc. We have performed a similar analysis on a range of scales and find this to be the range where the distribution is the most sensitive.

Selecting for objects in a dense environment increases the probability of having $N_{subs} = 2$ or more increases by almost 25%, from 9% to just over 11%. The effect gets stronger for hosts with larger values of N_{subs}. The Milky Way is somewhat overdense on this scale, having a massive companion M31 and a number of dwarf galaxies with total mass of roughly $(3-4) \times 10^{12}h^{-1}{\rm M}_\odot$ (once the mass of the Milky Way itself is excluded:Li et al. 2009). Even if all neighboring objects other than M31 are excluded, this puts the Milky Way in the top quartile of our measured mass distribution in Bolshoi. We can understand this by making an explicit cut for halos having nearby neighbors with $M_{\rm vir} = (1-3) \times 10^{12}{\rm M}_\odot$ (green points), which boosts the $N_{subs} = 2$ probability by roughly 2-σ. Thus, the local environment around the MW, which is dominated by the presence of M31, boosts the chance of seeing the Magellanic Clouds in the Milky Way.

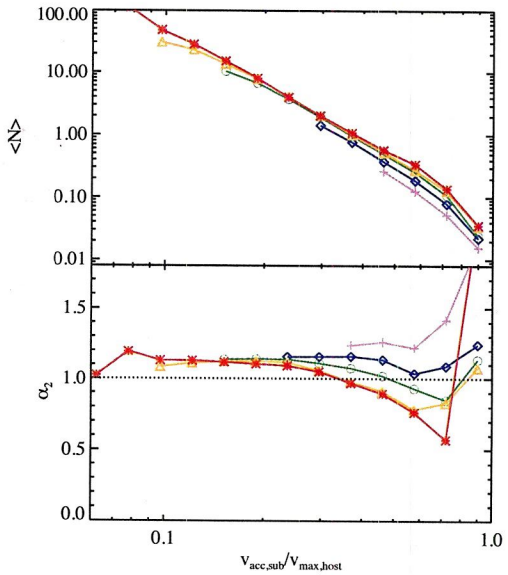

FIG. 3.— *Top Panel:* The trend of the best-fit value for $\langle N \rangle$ to the v_{acc} distribution function for hosts of varying masses. This is equivalent to the subhalo mass function. Cyan pluses, blue diamonds, green circles, and red triangles represent hosts with v_{max} = 200, 300, 600, and 1000 km s^{-1}, respectively. The white solid line shows the best fit to the proposed mass function from Boylan-Kolchin et al. (2010). *Bottom Panel:* The trend of the scatter in the distribution of the number of subhalos above a mass threshold. The dashed line represents $\alpha_2 = 1$, where the negative binomial distribution reduces to Poisson.

mass objects are able to form in both unbiased regions, and regions near to higher mass halos, creating a larger scatter in their subhalo populations. While not shown, we have made analogous plots to Figure 2 for hosts of higher mass and confirm that these objects typically have a weaker environmental impact on their subhalo populations.

It is also interesting to note that previous studies, in particular Kravtsov et al. (2004) and Boylan-Kolchin et al. (2010), have not seen such a trend. There are a number of possible explanations accounting for this, which include the improved h^{-1}kpc force resolution and $(250h^{-1}\text{Mpc})^3$ volume of the Bolshoi simulation, which allows for both better statistics more accurate tracking of subhalos as they orbit around their hosts. The increased volume of Bolshoi is particularly important if the trend is driven by halo environment, since a larger volume is necessary to probe a full range of environments. Hints of this trend, however, can be noticed in Figure 9 of Boylan-Kolchin et al. (2010).

While not shown, nearly identical trends in $\langle N \rangle$ and α_2 persist if we consider the mass ratio $v_{max,sub}/v_{max,host}$, using the maximum circular velocity of the subhalo at $z = 0$ instead of at the time of accretion.

To summarize, in this section, we have shown that satellites comparable in size to the LMC and SMC are relatively rare in Milky Way mass objects, occurring in roughly 9% of the potential hosts. Their abundance is dependent on a number of host properties, such as the host mass and environment, which can provide a boost at the 25% level. The proximity of M31 puts the Milky Way in a higher density environment, where we expect to see this boost, pushing the likelihood of an LMC/SMC pair up to 12%. Finally, it was shown that for massive subhalos, the scatter in the expected number of subhalos systematically increases with host mass. This is likely related to the environmental variations previously observed, where lower mass halos are able to form in a wider range of environments than higher mass objects.

In the next section we turn to the task of comparing our simulation results with observations from the SDSS, which requires the adoption of an abundance-matching algorithm for adding magnitudes to simulated galaxies.

4. SATELLITE STATISTICS FOR GALAXIES

We turn next to the issue of comparing these results with observational constraints. The classical satellite galaxies around the Milky Way have been well studied, and it is believed that we have a complete census of all objects brighter than $M_V \sim -6$ inside the virial radius of the Milky Way (Koposov et al. 2008; Tollerud et al. 2008). In particular, the two brightest objects, the LMC and SMC are 2-4 magnitudes dimmer than the Milky Way. The next brightest object, Sagittarius, is significantly dimmer, with $M_V = -13.1$, roughly 3 magnitudes dimmer than the SMC. From this, we can conservatively conclude that the census of objects brighter than $M_V = -16$ is complete.

4.1. *The Observational Sample*

The recent work of Liu et al. (2010) studied of the population of such LMC and SMC luminosity objects in SDSS. Here, Milky Way analogs were identified in the SDSS main sample by locating objects with $M_r = -21.2 \pm 0.2$ with no brighter companions within a cylinder of radius 500 kpc and length 1000 km s^{-1}. The abundance of satellite galaxies was then measured by counting the likelihood of having N_{subs} neighbors in the photometric sample with observed magnitudes 2-4 dimmer in a fixed 150 kpc aperture. The value for the SDSS r-band magnitude was determined using the K-correct code of Blanton & Roweis (2007) on a sample population of 500,000 SDSS galaxies. See Liu et al. (2010) for details.

4.2. *Modeling Galaxy Luminosities*

Because kinematic data is difficult to measure observationally (and, in the case of extragalactic satellite objects, presently impossible), the observations of Liu et al. (2010) cannot be directly compared to the results from the previous section, which determined abundances based on the v_{max} of the satellites. Instead, we employ a SubHalo Abundance Matching (SHAM) algorithm to our simulation to map magnitudes onto dark matter halos (Kravtsov et al. 2004; Conroy et al. 2006; Wetzel & White 2010; Behroozi et al. 2010b). Here, luminosities are assigned by matching the number density of observed objects brighter than a given luminosity with the number density of simulated objects greater than a given v_{max}. For subhalos, v_{max} at the time of accretion is used instead of the present $v_{max}(z = 0)$. We also impose a log-normal scatter between halo mass and luminosity. In our base model, we assume a scatter of 0.16 mag, consistent with constraints on larger group and cluster mass objects (More et al. 2009; Behroozi et al. 2010b).

This algorithm has been shown to be extremely successful in matching several statistical properties of the galaxy distribution, including the the luminosity dependence and redshift scaling of the two-point galaxy correlation function for galaxies brighter than $M_r < -19$ (Conroy et al. 2006), the galaxy-mass correlation function (Tasitsiomi et al. 2004), and

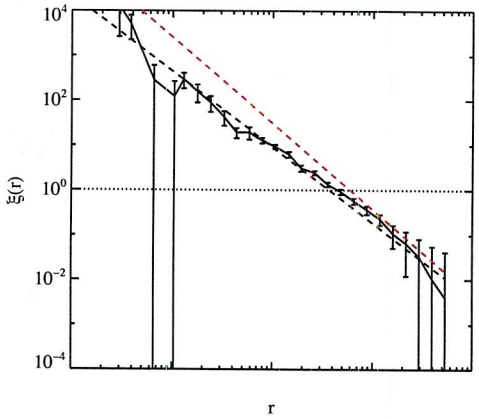

FIG. 6.— The 3D cross-correlation function, $\xi(r)_{\rm MW-MC}$, between Milky Way like hosts and all LMC and SMC magnitude satellite galaxies. The black dashed line represents a power-law fit to $\xi(r)$. For reference, the dotted red line denotes the auto-correlation between galaxies with $-21 < M_r - 5\log(h) = -20$ in SDSS DR7 as measured in The SDSS Collaboration et al. (2010).

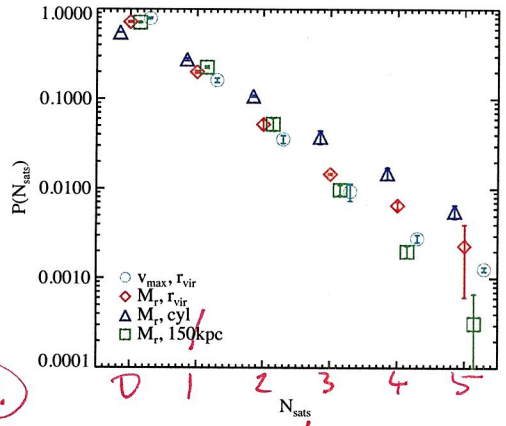

FIG. 7.— The probability of having N_{subs} LMC and SMC-type objects in simulations based on SHAM and v_{max} for various satellite definitions. The blue circles count objects with $v_{max} > 50$km s^{-1} within the virial radius, while the yellow triangles, red diamonds, and green boxes count objects 2-4 magnitudes dimmer than their host using a SHAM model with 0.16 dex scatter. The red diamonds were calculated using all objects inside the virial radius. The the blue and triangles and green boxes are equivalent to the two background subtractions used in Liu et al. (2010): a cylindrical apertures of radius 150 kpc and length 3.7 Mpc (blue triangles), and a fixed 150 kpc spherical apperture (green boxes).

Mpc/h and $\gamma = 1.9$ for the autocorrelation function of galaxies with $M_r = -20.7 - -21.7$. Coincidentally, this correlation scale is very similar to the size of the redshift-space distortions induced by the typical 110 km s^{-1} velocity dispersion predicted by a 10^{12}M$_\odot$ halo (Evrard et al. 2008). At $z = 0.08$, where the bulk of our simulated halos live, these distortions cause a roughly 4.7 Mpc smearing out of the halo satellite population. Since a cylinder of this length represents the most accurate measurements one could make for the number of subhalos around a host using spectroscopic data, we consider this to be an additional justification for considering all dimmer galaxies in such a cylinder to be satellites of a Milky Way analog in our simulation when comparing with the appropriate background subtraction method of Liu et al. (2010).

In Figure 7 we compare the results from a number of different definitions for a satellite galaxy: spherical and cylindrical apertures, as well as including satellites based on $v_{\rm max}$ and magnitude. The blue circles counted objects with $v_{max} = 50-80$km s^{-1} within the virial radius, while the red diamonds, blue triangles, and green boxes count objects 2-4 magnitudes dimmer than their host using a SHAM model with 0.16 dex scatter in luminosity at a given $v_{\rm max}$. The red diamonds were calculated using all objects inside the virial radius, while the blue triangles use cylindrical apertures of radius 150 kpc and length 5.3 Mpc, and the green boxes also use a spherical aperture of 150 kpc. These latter two definitions are our simulation equivalents to the two subtraction methods employed in Liu et al. (2010). All error bars were calculated using a jackknife method with 10 sub-regions.

Many trends are readily apparent for the relations of Figure 7. First, it is clear that the selection of objects based on $v_{\rm max}$ or our SHAM magnitudes has little impact on the values of the probability distribution. This should not be surprising because our model naturally imposes a magnitude $-16.7 < M_r < -18.6$ for objects with $v_{\rm max} = 50-80$km s^{-1}, the approximate limit of our magnitude cut when doing the SHAM comparison. More interesting to consider is the trend with changing cylinder size. Unsurprisingly, the green boxes representing satellites that are inside both the virial radius and a 150 kpc aperture are well below the yellow points representing all satellites inside the virial radius. This impact is surprisingly low at the 1-satellite level, and grows with N_{subs}, which indicates that the first satellite galaxy around a Milky Way-luminosity host is typically located near the center, while additional satellites reside more in the outskirts.

The yellow points in Figure 7, representing satellites inside a fixed cylinder size with radius 150 kpc and length 5.3 Mpc (the correlation length for the host-satellite cross correlation function in figure 6) demonstrate the impact of line-of-sight correlations, and is likely the best comparison with the uncorrected results from Liu et al. (2010). While we present the results from only a single cylinder length, the results are very insensitive to any length beyond $\sim$ 1Mpc, where the correlation function has dropped off significantly. Varying the cylinder length from 2 – 8 Mpc typically changes our results roughly five percent, comparable to the size of our error bars. Thus, the comparison seems robust. Even though this measurement is done using a fixed aperture of 150 kpc, these line-of-sight correlations boost the probability of seeing a single satellite above what is measured using the proper subhalo definition of an object inside the virial radius.

Liu et al. (2010) also present a second method of background subtraction, measuring the noise profile using an annulus with equal surface area to the 150 kpc aperture. This second method for background subtraction should effectively measure the noise due to both the random background as well as correlated structures. This presents us with a second method for comparing our simulated results their observations, by measuring $P(N_{subs})$ for subhalos within a sphere of radius 150 kpc around our MW-like objects. The results from this calculation can be seen as the green points in Figure 7. As expected from our measurements of the cross correlation function, these probabilities lie below the measurements using either the virial radius or our 5.3 x 0.15 Mpc cylinder. The mean virial radius for our halos is a little less than 300 kpc, and it is interesting to note that the cumulative probability for hosting once satellite differs by less than 5% when calculated using the virial radius instead of 150 kpc, while this difference increases rapidly for higher N_{subs}'s. This seems to indicate that

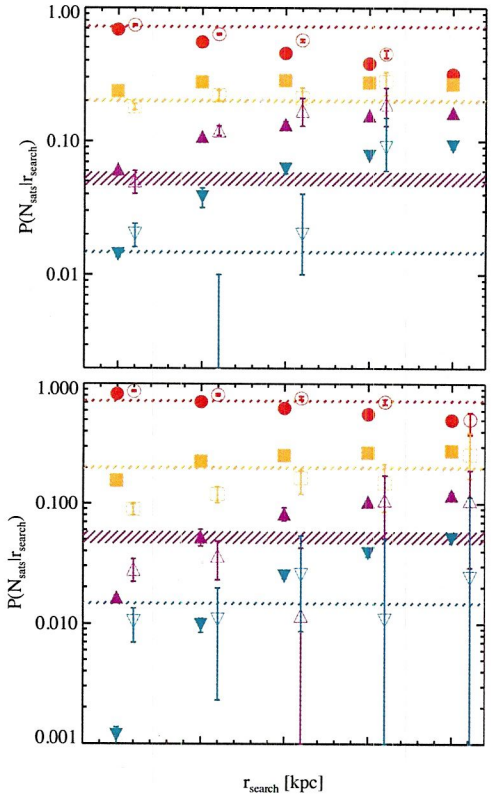

FIG. 9.— Abundances of LMC and SMC-type objects in the simulation, as a function of search radius. In call cases the fi lled symbols were calculated using Bolshoi+SHAM, while the open symbols represent SDSS measurements from Liu et al. (2010). Here, the red circles, orange squares, magenta triangles, and cyan inverse-triangles represent the probability for a Milky Way like galaxy to have 0, 1, 2, or 3 subhalos, respectively. For the Bolshoi objects, the probabilities were calculated using a fi xed cylindrical aperture with radius 150 kpc and length 5.3 Mpc. The cylinder-size values for the SDSS sample have been offset by 10 kpc for clarity. The hatched lines represent the probabilities for hosting N_{subs} subhalos inside the virial radius of the host.

ing with them their richer subhalo populations. As we shall discuss in the next section, this has the effect of creating a tail to the negative-binomial distribution that sets the probability for a host to have N_{subs} subhalos.

(again, need to re-calibrate for Mr instead of Mr - 5 log 5) It is also worth noting that the dark blue points representing a scatter of $\sigma = 0.3$ look to be violating the trend of an increasing high-N_{subs} probability. This is not due to any special behavior in this regime, but more represents the limits of our simulation resolution. As scatter increases, objects with $M_r - 5\log h > -16.5$, which nominally have $v_{acc} = 90$km/s using a scatter-free SHAM, have infall masses as low as 65 km/s in our $\sigma = 0.3$ model, dangerously close to the Bolshoi completeness limit of 50 km/s. Combined with stripping of objects once they accrete onto their host halos, we expect to be losing potentially 10-15% of the satellite population when we push scatter this high. It's important to take a moment to use this to appreciate the high levels of resolution necessary to fully model a galaxy population using SHAM. While a scatter of $\sigma = 0.3$ is likely ruled out in the data, if such scatter were appropriate the Bolshoi simulation would only be able to populate galaxies down to $M_r \sim -17.5$ to avoid losing fewer than 10% of the objects.

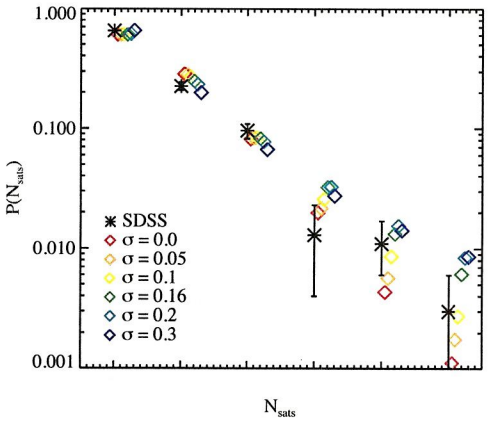

FIG. 10.— Dependence of satellite probabilities on scatter in the relationship between halo mass and galaxy luminosity. In each case, the model assumes a constant value of σ corresponding to the scatter in log L at a given v_{acc}. Larger scatter values tend to have more systems with many satellites, largely because more high mass hosts are scattered into the sample.

5. STATISTICS OF SATELLITES IN LUMINOSITY-SELECTED HOSTS

As noted previously, the inclusion of scatter creates a significant tail in the probability distribution for a host to have N_{subs} satellite galaxies. Consequently, the negative binomial distribution that was found to describe the $P(N)$ distribution for a host halo does not produce a good fit when applied to galaxies. Additionally, the change in star formation efficiency with host halo mass breaks the self-similarity that was observed for host halos (Behroozi et al. 2010b, and references therein). In this section, we re-investigate the issue of quantifying the probability distribution $P(N)$ for a galaxy to have N_{subs} satellite galaxies within its virial radius.

In Figure 11, we show a series of probability distributions for a $M_r = -20.5 - 5\log h$ galaxy to host N_{subs} subhalos brighter than -19, -17.5 and -16. This plot was generated using a scatter of $\sigma = 0.16$. A low probability tail clearly extends to high N_{subs} where it was previously absent when considering v_{max}-selected hosts. This is emphasized by the shape of the dotted lines, which present the best fitting binomial distributions. While at first glance this tail seems to have too low of a probability for us to be seriously worried about fitting it, we will see below that the tail becomes significantly more important when considering brighter, higher-mass hosts.

As a better fit, we present a modified binomial distribution by adding a power law tail,

$$P(N|r,p,T,\tau) = \frac{\Gamma(n+r)}{\Gamma(r)\Gamma(n+1)} p^r (1-p)^n + Te^{-\tau n}, \qquad (7)$$

where r and p are defined in Equation 5 and T and τ control the size of the high-N tail that comes about as a result of scatter in the mass–luminosity relation. The dashed lines in Figure 11 show the best fits to Equation 7, which has a significantly improved fit to the simulation (albeit at the expense of adding two new parameters). While we do not investigate this further, it is worth noting that changing the scatter in our SHAM model has a direct impact on T and τ. High values of scatter will have a more pronounced tail, which will cause both the amplitude and slope of this tail to increase. For the rest of this work, we will limit ourselves to using a model with $\sigma = 0.16$.

While we could present our best-fitting parameters to model

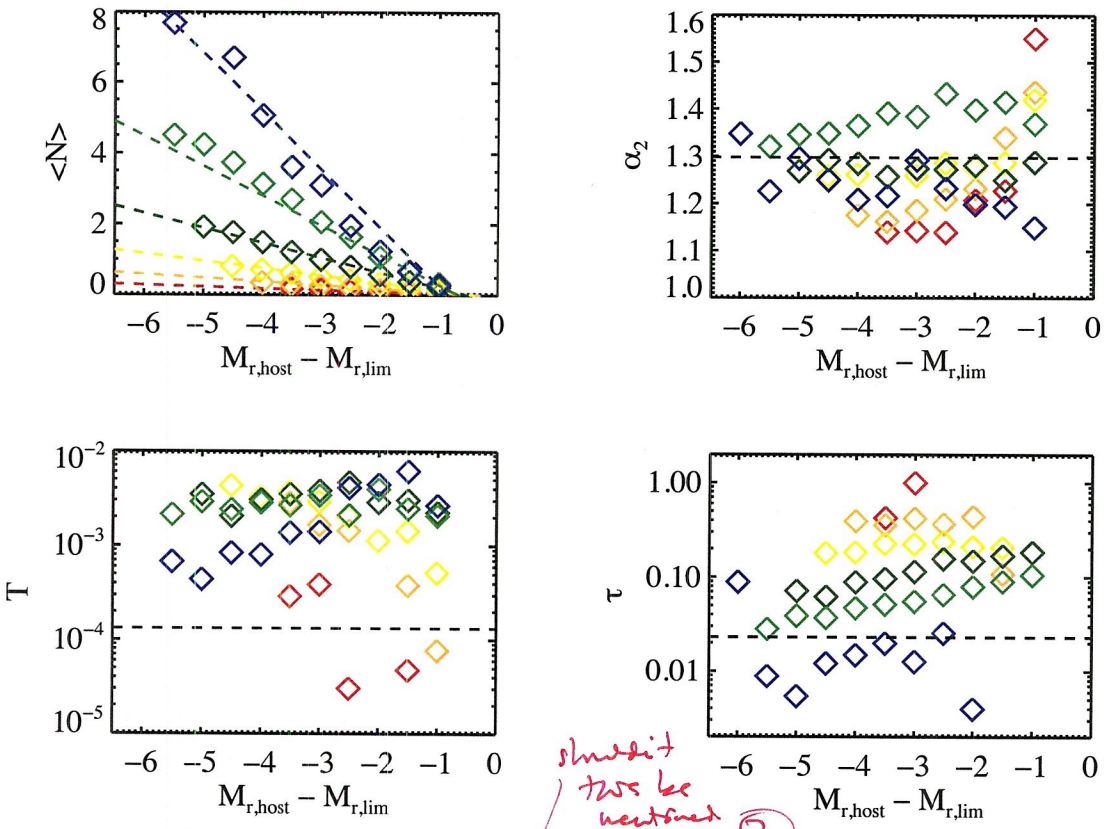

FIG. 12.— Dependence of fit parameters specifying the P(N) distribution on the difference between host and satellite magnitude. Parameters are fit to a negative binomial plus power law distribution, as given by Equation 7. Different colored points represent hosts of different masses: blue, green, dark green, yellow, orange, and red points are hosts with $M_t = -19.5, -20, -20.5, -21, -21.5$, and $-22 - 5\log h$. Dashed lines represent fits to the distribution as given by Equation 8.

as the SMC, whether we define our objects according to mass or magnitude. These results confirm the outlines of previous simulation results (e.g. Boylan-Kolchin et al. 2010) using a volume 100 times larger and given a more direct comparison with observables. They are also in excellent agreement with observational results (Liu et al. 2010; James & Ivory 2010), including the full probability distribution of satellites found by L10. This result has a number of implications.

First, this is a validation of the ΛCDM paradigm down to the level of $10^{10}h^{-1}M_\odot$ objects. At this level, there is no indication that our standard picture of galaxy formation breaks down. One common criticism of this method is that, perhaps SHAM is so robust as to *always* produce the correct answer. While this is something to be concerned about, it is important to keep track of the exact assumptions of SHAM. First and foremost, SHAM assumes that mass is the only parameter that sets the properties of a galaxy. While it is robust to, i.e., a constantly changing star formation efficiency with halo mass, such a comparison as presented here will break down if there is any sort of environmental dependence. That is, if subhalos of a given mass evolve differently than objects of the same mass in the field, SHAM should not produce good agreement.

We do see some manifestations of assembly bias with regards to the dark matter subhalo population inside of Milky Way mass galaxies. Here, we find that halos in higher density regions likely host more massive subhalos than those in lower density regions. This effect appears to be most pronounced for local measurements of density, and suggests that our proximity to M31 boosts the likelihood for us to see a LMC/SMC pair by about 25%. It is interesting that this result is in qualitative agreement with the work of Ishiyama et al. (2009b), who saw a similar trend with environment but claimed it was most sensitive at the $\sim 5h^{-1}$Mpc scale. They note that we are in an underdense region on these scales, and cite this as a possible ingredient for solving the missing satellite problem. While our simulations do not let us comment on objects smaller than the Magellanic Clouds, if our observed trend were extrapolated down to lower masses it would result in an *opposite* effect, where the presence of M31 could serve to exacerbate the missing satellite problem.

We have presented a prediction for the probability distribution of satellite number, $P(N)$, as a function of host and satellite magnitude. This can already be tested with current data over a wide range, which would provide a non-trivial test of our model. Deviations from Poisson satellite number may have consequences for HOD modeling.

RHW and MTB were supported by the National Science Foundation under grant NSF AST-0807312. We thank Louie Strigari and Lulu Liu for useful discussions.

REFERENCES

Abazajian, K. N., Adelman-McCarthy, J. K., Agüeros, M. A., Allam, S. S., Allende Prieto, C., An, D., Anderson, K. S. J., Anderson, S. F., Annis, J., Bahcall, N. A., & et al. 2009, ApJS, 182, 543

Battaglia, G., Helmi, A., Morrison, H., Harding, P., Olszewski, E. W., Mateo, M., Freeman, K. C., Norris, J., & Shectman, S. A. 2005, MNRAS, 364, 433

Koposov, S. E., Yoo, J., Rix, H., Weinberg, D. H., Macciò, A. V., & Escudé, J. M. 2009, ApJ, 696, 2179
Kravtsov, A. V., Berlind, A. A., Wechsler, R. H., Klypin, A. A., Gottlöber, S., Allgood, B., & Primack, J. R. 2004, ApJ, 609, 35
Kravtsov, A. V., Klypin, A. A., & Khokhlov, A. M. 1997, ApJS, 111, 73
Lacey, C. & Cole, S. 1993, MNRAS, 262, 627
Li, Y., Helmi, A., De Lucia, G., & Stoehr, F. 2009, MNRAS, 397, L87
Libeskind, N. I., Cole, S., Frenk, C. S., Okamoto, T., & Jenkins, A. 2007, MNRAS, 374, 16
Liu, L., Gerke, B., Wechsler, R., Behroozi, P., & Busha, M. 2010, ApJ, to be submitted
Madau, P., Diemand, J., & Kuhlen, M. 2008, ApJ, 679, 1260
Marín, F. A., Wechsler, R. H., Frieman, J. A., & Nichol, R. C. 2008, ApJ, 672, 849
Moore, B., Ghigna, S., Governato, F., Lake, G., Quinn, T., Stadel, J., & Tozzi, P. 1999, ApJ, 524, L19
More, S., van den Bosch, F. C., Cacciato, M., Mo, H. J., Yang, X., & Li, R. 2009, MNRAS, 392, 801
Okamoto, T., Frenk, C. S., Jenkins, A., & Theuns, T. 2010, MNRAS, 406, 208
Smith, M. C., Ruchti, G. R., Helmi, A., Wyse, R. F. G., Fulbright, J. P., Freeman, K. C., Navarro, J. F., Seabroke, G. M., Steinmetz, M., Williams, M., Bienaymé, O., Binney, J., Bland-Hawthorn, J., Dehnen, W., Gibson, B. K., Gilmore, G., Grebel, E. K., Munari, U., Parker, Q. A., Scholz, R., Siebert, A., Watson, F. G., & Zwitter, T. 2007, MNRAS, 379, 755
Springel, V., Wang, J., Vogelsberger, M., Ludlow, A., Jenkins, A., Helmi, A., Navarro, J. F., Frenk, C. S., & White, S. D. M. 2008, MNRAS, 391, 1685
Springel, V., White, S. D. M., Tormen, G., & Kauffmann, G. 2001, MNRAS, 328, 726
Stadel, J., Potter, D., Moore, B., Diemand, J., Madau, P., Zemp, M., Kuhlen, M., & Quilis, V. 2009, MNRAS, 398, L21
Stanimirović, S., Staveley-Smith, L., & Jones, P. A. 2004, ApJ, 604, 176
Tasitsiomi, A., Kravtsov, A. V., Wechsler, R. H., & Primack, J. R. 2004, ApJ, 614, 533
The SDSS Collaboration, Zehavi, I., Zheng, Z., Weinberg, D. H., Blanton, M. R., Bahcall, N. A., Berlind, A. A., Brinkmann, J., Frieman, J. A., Gunn, J. E., Lupton, R. H., Nichol, R. C., Percival, W. J., Schneider, D. P., Skibba, R. A., Strauss, M. A., Tegmark, M., & York, D. G. 2010, ArXiv e-prints
Tollerud, E. J., Bullock, J. S., Strigari, L. E., & Willman, B. 2008, ApJ, 688, 277
Trujillo-Gomez, S., Klypin, A., Primack, J., & Romanowsky, A. J. 2010, ArXiv e-prints
van der Marel, R. P., Alves, D. R., Hardy, E., & Suntzeff, N. B. 2002, AJ, 124, 2639
Wechsler, R. H., Bullock, J. S., Primack, J. R., Kravtsov, A. V., & Dekel, A. 2002, ApJ, 568, 52
Wetzel, A. R. & White, M. 2010, MNRAS, 403, 1072
Xue, X. X., Rix, H. W., Zhao, G., Re Fiorentin, P., Naab, T., Steinmetz, M., van den Bosch, F. C., Beers, T. C., Lee, Y. S., Bell, E. F., Rockosi, C., Yanny, B., Newberg, H., Wilhelm, R., Kang, X., Smith, M. C., & Schneider, D. P. 2008, ApJ, 684, 1143
York, D. G., Adelman, J., Anderson, Jr., J. E., Anderson, S. F., Annis, J., Bahcall, N. A., Bakken, J. A., Barkhouser, R., Bastian, S., Berman, E., Boroski, W. N., Bracker, S., Briegel, C., Briggs, J. W., Brinkmann, J., Brunner, R., Burles, S., Carey, L., Carr, M. A., Castander, F. J., Chen, B., Colestock, P. L., Connolly, A. J., Crocker, J. H., Csabai, I., Czarapata, P. C., Davis, J. E., Doi, M., Dombeck, T., Eisenstein, D., Ellman, N., Elms, B. R., Evans, M. L., Fan, X., Federwitz, G. R., Fiscelli, L., Friedman, S., Frieman, J. A., Fukugita, M., Gillespie, B., Gunn, J. E., Gurbani, V. K., de Haas, E., Haldeman, M., Harris, F. H., Hayes, J., Heckman, T. M., Hennessy, G. S., Hindsley, R. B., Holm, S., Holmgren, D. J., Huang, C., Hull, C., Husby, D., Ichikawa, S., Ichikawa, T., Ivezić, Ž., Kent, S., Kim, R. S. J., Kinney, E., Klaene, M., Kleinman, A. N., Kleinman, S., Knapp, G. R., Korienek, J., Kron, R. G., Kunszt, P. Z., Lamb, D. Q., Lee, B., Leger, R. F., Limmongkol, S., Lindenmeyer, C., Long, D. C., Loomis, C., Loveday, J., Lucinio, R., Lupton, R. H., MacKinnon, B., Mannery, E. J., Mantsch, P. M., Margon, B., McGehee, P., McKay, T. A., Meiksin, A., Merelli, A., Monet, D. G., Munn, J. A., Narayanan, V. K., Nash, T., Neilsen, E., Neswold, R., Newberg, H. J., Nichol, R. C., Nicinski, T., Nonino, M., Okada, N., Okamura, S., Ostriker, J. P., Owen, R., Pauls, A. G., Peoples, J., Peterson, R. L., Petravick, D., Pier, J. R., Pope, A., Pordes, R., Prosapio, A., Rechenmacher, R., Quinn, T. R., Richards, G. T., Richmond, M. W., Rivetta, C. H., Rockosi, C. M., Ruthmansdorfer, K., Sandford, D., Schlegel, D. J., Schneider, D. P., Sekiguchi, M., Sergey, G., Shimasaku, K., Siegmund, W. A., Smee, S., Smith, J. A., Snedden, S., Stone, R., Stoughton, C., Strauss, M. A., Stubbs, C., SubbaRao, M., Szalay, A. S., Szapudi, I., Szokoly, G. P., Thakar, A. R., Tremonti, C., Tucker, D. L., Uomoto, A., Vanden Berk, D., Vogeley, M. S., Waddell, P., Wang, S., Watanabe, M., Weinberg, D. H., Yanny, B., & Yasuda, N. 2000, AJ, 120, 1579
Zentner, A. R., Berlind, A. A., Bullock, J. S., Kravtsov, A. V., & Wechsler, R. H. 2005, ApJ, 624, 505
Zentner, A. R. & Bullock, J. S. 2003, ApJ, 598, 49

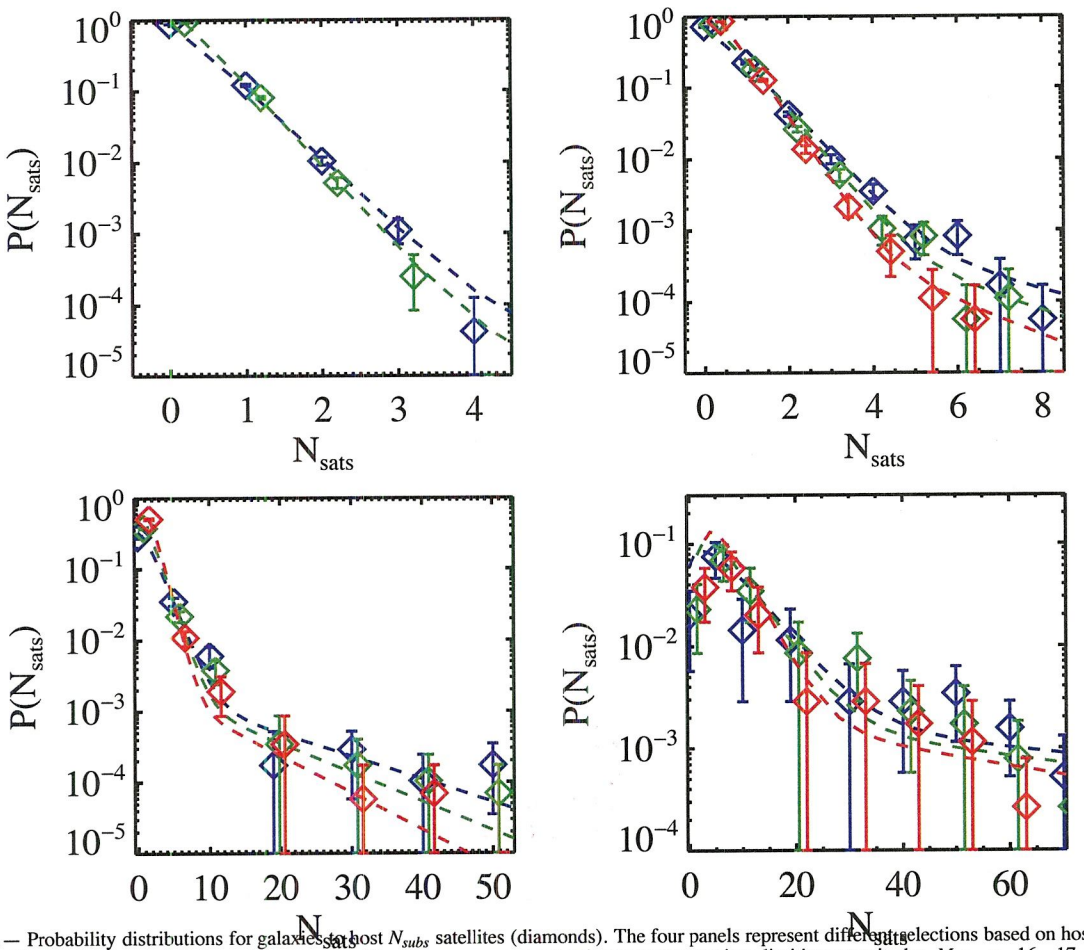

FIG. 13.— Probability distributions for galaxies to host N_{subs} satellites (diamonds). The four panels represent different selections based on host mass, $M_{r,host}$ = −19, −20, −21, −22 for the top left through lower right. The blue, green, and red points represent various limiting magnitudes, $M_{r,lim}$ = −16, −17, −18. The dashed lines represent our model with fi t parameters from Eq. 8 and table 5.

Behroozi, P. S., Busha, M., Wechsler, R. H., et al. 2010a, in preparation
Behroozi, P. S., Conroy, C., & Wechsler, R. H. 2010b, ApJ, 717, 379
Besla, G., Kallivayalil, N., Hernquist, L., Robertson, B., Cox, T. J., van der Marel, R. P., & Alcock, C. 2007, ApJ, 668, 949
Blanton, M. R., Hogg, D. W., Bahcall, N. A., Brinkmann, J., Britton, M., Connolly, A. J., Csabai, I., Fukugita, M., Loveday, J., Meiksin, A., Munn, J. A., Nichol, R. C., Okamura, S., Quinn, T., Schneider, D. P., Shimasaku, K., Strauss, M. A., Tegmark, M., Vogeley, M. S., & Weinberg, D. H. 2003, ApJ, 592, 819
Blanton, M. R. & Roweis, S. 2007, AJ, 133, 734
Blanton, M. R., Schlegel, D. J., Strauss, M. A., Brinkmann, J., Finkbeiner, D., Fukugita, M., Gunn, J. E., Hogg, D. W., Ivezić, Ž., Knapp, G. R., Lupton, R. H., Munn, J. A., Schneider, D. P., Tegmark, M., & Zehavi, I. 2005, AJ, 129, 2562
Blumenthal, G. R., Faber, S. M., Primack, J. R., & Rees, M. J. 1984, Nature, 311, 517
Boylan-Kolchin, M., Springel, V., White, S. D. M., & Jenkins, A. 2010, MNRAS, 406, 896
Bullock, J. S., Kolatt, T. S., Sigad, Y., Somerville, R. S., Kravtsov, A. V., Klypin, A. A., Primack, J. R., & Dekel, A. 2001, MNRAS, 321, 559
Busha, M. T., Evrard, A. E., & Adams, F. C. 2007, ApJ, 665, 1
Busha, M. T., Marshall, P., & Wechsler, R. H. 2010, in preparation
Chen, J., Kravtsov, A. V., Prada, F., Sheldon, E. S., Klypin, A. A., Blanton, M. R., Brinkmann, J., & Thakar, A. R. 2006, ApJ, 647, 86
Conroy, C., Wechsler, R. H., & Kravtsov, A. V. 2006, ApJ, 647, 201
Dehnen, W., McLaughlin, D. E., & Sachania, J. 2006, MNRAS, 369, 1688
Diemand, J., Moore, B., & Stadel, J. 2004, MNRAS, 352, 535
Evrard, A. E., Bialek, J., Busha, M., White, M., Habib, S., Heitmann, K., Warren, M., Rasia, E., Tormen, G., Moscardini, L., Power, C., Jenkins, A. R., Gao, L., Frenk, C. S., Springel, V., White, S. D. M., & Diemand, J. 2008, ApJ, 672, 122
Gao, L., Frenk, C. S., Boylan-Kolchin, M., Jenkins, A., Springel, V., & White, S. D. M. 2010, ArXiv e-prints
Gao, L., White, S. D. M., Jenkins, A., Stoehr, F., & Springel, V. 2004, MNRAS, 355, 819
Gnedin, O. Y., Brown, W. R., Geller, M. J., & Kenyon, S. J. 2010, ApJ, 720, L108
Harris, J. & Zaritsky, D. 2006, AJ, 131, 2514
Ishiyama, T., Fukushige, T., & Makino, J. 2009a, ApJ, 696, 2115
—. 2009b, ApJ, 696, 2115
James, P. A. & Ivory, C. F. 2010, ArXiv e-prints
Kallivayalil, N., van der Marel, R. P., & Alcock, C. 2006a, ApJ, 652, 1213
Kallivayalil, N., van der Marel, R. P., Alcock, C., Axelrod, T., Cook, K. H., Drake, A. J., & Geha, M. 2006b, ApJ, 638, 772
Klypin, A. & Holtzman, J. 1997, ArXiv Astrophysics e-prints
Klypin, A., Kravtsov, A. V., Valenzuela, O., & Prada, F. 1999, ApJ, 522, 82
Klypin, A., Trujillo-Gomez, S., & Primack, J. 2010, ArXiv e-prints
Komatsu, E., Smith, K. M., Dunkley, J., Bennett, C. L., Gold, B., Hinshaw, G., Jarosik, N., Larson, D., Nolta, M. R., Page, L., Spergel, D. N., Halpern, M., Hill, R. S., Kogut, A., Limon, M., Meyer, S. S., Odegard, N., Tucker, G. S., Weiland, J. L., Wollack, E., & Wright, E. L. 2010, ArXiv e-prints
Koposov, S., Belokurov, V., Evans, N. W., Hewett, P. C., Irwin, M. J., Gilmore, G., Zucker, D. B., Rix, H.-W., Fellhauer, M., Bell, E. F., & Glushkova, E. V. 2008, ApJ, 686, 279

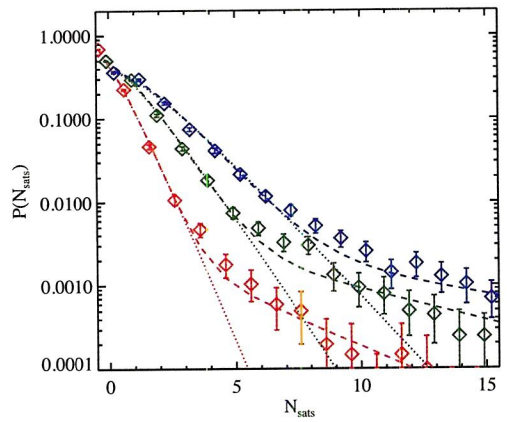

FIG. 11.— Probability of hosting N_{subs} satellite galaxies in a Milky Way-luminosity host, for various satellite selection criteria. The red, green, and blue points represent satellites brighter than $M_r = -19, -17.5$, and -16. Dotted lines represent the best fit negative binomial distribution, while the dashed line shows the best fit negative binomial plus power-law distribution.

the distributions in Figure 11, a much more useful process would be to model the general $P(N)$ distribution as a function of both host magnitude and limiting satellite magnitude, as implied by Figure 1. Unfortunately, this proves to be much more difficult to do for galaxies than for halos. As discussed extensively, because the power spectrum is mostly featureless, in the relative regime, halos typically look like scaled versions of other halos. While there are correlations between halo properties, such as the mean mass-concentration and mass-formation time relations (e.g. Bullock et al. 2001; Wechsler et al. 2002; Busha et al. 2007), these are more generally secondary effects that without a terribly strong impact on bulk halo properties. As an example of this, the top panel of Figure 3, which shows the mean number of satellites above a given mass cut for mass-selected host halos exhibits a power-law behavior with identical parameters regardless of the host mass. This is not the case for magnitude-selected objects.

(need to re-do the plot/constraints using Mr instead of Mr - 5 logh) Figure 12 presents our general fits for the $P(N_{subs})$ distribution to Equation 7 around magnitude-selected halos for several magnitude thresholds, down to an arbitrary luminosity ratio (magnitude difference). As can be clearly seen in, i.e., the top left panel which shows the trend of the mean number of satellite galaxies ($\langle N \rangle$) as a function of luminosity ratio, galaxies do not scale self-similarly — brighter objects are significantly more likely to host N_{subs} satellites at a given mass ratio than dimmer galaxies. This is a manifestation of the varying star formation efficiency with halo mass as seen in, e.g. Figure 2 of Behroozi et al. (2010b). The stellar mass-halo mass ration, $M_{star}(M_{halo})$, has a monotonically decreasing positive-definite slope. This means that, from the dark matter standpoint, while the satellites of $10^{14}M_\odot$ host halos are just scaled version of the satellites around a $10^{12}M_\odot$ object, the galaxy populations in those halos do not scale in the same way. In particular, relative to their host luminosities, the satellites around the $10^{14}M_\odot$ halo will be brighter than the satellites around the $10^{12}M_\odot$ halo. Thus, while the $\langle N \rangle$ values for mass-selected satellites lie on a single line in Figure 3, luminosity-selected halos do not scale in such a manner, giving us the changing lines in the top left panel of Figure 12: brighter host galaxies have more satellites at a fixed luminosity ratio, L_{sat}/L_{host}, than dimmer hosts.

TABLE 2
PARAMETERS SPECIFYING $P(N)$ DISTRIBUTION IN EQ. 10

parameter	best-fit value
$N_{0,a}$	-54
$N_{0,b}$	40
$N_{1,a}$	-39
$N_{1,b}$	29
$\alpha_{2,0}$	1.3
T_0	1.3×10^{-4}
τ_0	0.023

The trends in τ can also be readily understood though simple scaling relations. First, consider a fixed luminosity ratio, $|M_{r,host} - M_{r,lim}|$. Since brighter hosts correspond to more massive halos, these objects live in a steeper part of the mass function, where a fixed scatter creates a broader selection of host masses, the larger of which are more likely to host bright satellites. Because of this, the exponential tail falls off more slowly, resulting in a lower τ. The trend of τ increasing with luminosity ratio for a fixed host mass

Guided by these observations, and noting that α and T don't have strong trends with either host magnitude or limiting luminosity ratio, we propose a 7-parameter fit to generally describe the full $P(N|M_{r,host}, M_{r,lim})$. We use our generalized negative-binomial plus power law as defined in Equation 7, but parameterize $\langle N \rangle$ with a linear fit whose both slope and offset depend on host magnitude, a constant α, T, and τ. While our nominal fit can be improved using a τ that is a power-law in $M_{r,host} - M_{r,lim}$ with a normalization that depends on host mass, the actual fit does not significantly improve the formal χ^2, so we elect to hold it constant. Our full fit for Equation 7 then becomes a function of the parameters $N_{0.a}, N_{0,b}, N_{1,a}, N_{1,b}, \alpha_{2,0}, T_0$, and τ_0 defined by:

$$P(N|M_{r,host}, M_{r,lim}) = \frac{\Gamma(n+r)}{\Gamma(r)\Gamma(n+1)} p^r (1-p)^n + T_0 e^{-\tau_0 n} \quad (8)$$

where

$$p = \frac{1}{1 + (\alpha_{2,0}\langle N \rangle)}$$
$$r = \frac{1}{\alpha_{2,0}^2 - 1} \quad (9)$$
$$\langle N \rangle = -10^{N_{0,a} + N_{0,b} * \log(M_{r,host})} - (M_{r,host} - M_{r,lim}) 10^{N_{1,a} + N_{1,b} * \log(M_{r,host})}.$$

Fitting over all host halos down to $M_r = -19 - 5\log h$ and their satellites down to $M_r = -16 - 5\log h$ in Bolshoi, we come up with the best fitting parameters for Equation 10 and present them in table 5. As a final validation of this result, Figure 13 shows the measured $P(N)$ distributions for a range of $M_{r,host}$ and $M_{r,lim}$'s, along with the distribution from our model in Eq. 8.

6. CONCLUSIONS AND SUMMARY

In this work, we have examined the likelihood for simulated MW-like dark matter halos to host substructures similar to the Magellanic Clouds. We have done this analysis using both dark matter kinematic information, as well as an abundance-matching technique that assigns galaxy luminosities to resolved dark matter halos and allows direct comparison with observations. The main result of this work is that MW-like objects have a roughly 5% chance to host two subhalos as big

TABLE 1
PROBABILITY OF HOSTING N_{subs} SATELLITE GALAXIES BRIGHTER THAN $M_{r,host}$ +4 AROUND A MILKY WAY MAGNITUDE HOST HALO WITHIN VARIOUS APERTURES.

	r_{vir}^{a}	cylinder	sphere
$P(0)$	$72 \pm 2\%$	$55 \pm 1\%$	$71 \pm 1\%$
$P(1)$	$20 \pm 1\%$	$28 \pm 1\%$	$23 \pm 1\%$
$P(2)$	$5.2 \pm 1\%$	$11 \pm 1\%$	$5.2 \pm 0.2\%$
$P(3)$	$1.5 \pm 0.3\%$	$3.8 \pm 0.6\%$	$1.0 \pm 0.1\%$
$P(4)$	$0.65 \pm 0.6\%$	$1.5 \pm 0.3\%$	$0.2 \pm 0.1\%$

[a] r_{vir} refers to halos contained within the virial radius of the host, cylinder refers to objects within a cylinder with radius 150 kpc and length 5.2 Mpc, and sphere refers to objects within a sphere of radius150 kpc

the first subhalo for a MW-like halo typically lives close to the halo center, while additional ones live at preferentially higher radii. The numerical values for many of these probabilities are presented in Table 4.4. Note that, while we are only counting objects as satellites if they are 2-4 magnitudes dimmer than their hosts for the most accurate comparison with L10, these numbers are essentially identical to considering a threshold sample of objects 0-4 magnitudes dimmer than their hosts. Changing this definition creates only percent-level changes, well within the statistical error bars.

4.4. *Comparisons Between Simulations and Observations*

Figure 8 shows the main result of our analysis, making direct comparison with the results of Liu et al. (2010). Here, we plot their $P(N_{subs})$ measurements (black stars) and compare directly with our SHAM results using both our definition of all subhalos within the virial radius (yellow triangles) and objects inside a fixed cylinder with radius 150 kpc and length 5.3 Mpc (red diamonds). The agreement here is rather striking. At no N_{subs} do the two results differ by more than $\sim 1\sigma$, and in most situations the two simulation results (inside the virial radius and a fixed cylinder) bracket measurements. We take this to indicate a success for both the ΛCDM and SHAM models, particularly indicating, with excellent statistics, that the HOD predicted by Bolshoi for Milky Way-like objects at the massive end perfectly matches observations, and there is no evidence for either a missing or excess satellite problem.

(Just got 150 sphere subtraction from Lulu. Will make same plots and add) Looking into more detail at the SDSS/Bolshoi comparisons, we can further investigate the dependence of $P(N_{subs})$distribution on the aperture size, as done in Liu et al. (2010). For this, we look at the probability of finding N_{subs}satellite galaxies in a cylindrical aperture around their host, where the cylinder has a constant length of 5.3 Mpc, and the radius is varied from 100 to 250 kpc. The results are shown in Figure 9. Here, the red circles, orange squares, magenta triangles, and cyan inverse-triangles represent the probability of having 0, 1, 2, or 3 subhalos. Open symbols represent SDSS measurements, while filled symbols come from our Bolshoi+SHAM model. Again, we see excellent agreement between simulations and observations. In general, higher valules of N_{subs}seem to have the worst agreement at all radii. This is potentially due to difficulties in making an accurate background subtraction when doing this calculation in observations.

Figure 9 also shows the probability for hosting N_{subs} satellites inside the virial radius of Milky Way-like galaxies. We can use this as an additional condition to understand the appropriate cylinder radius for most closely ~~matching~~ matching

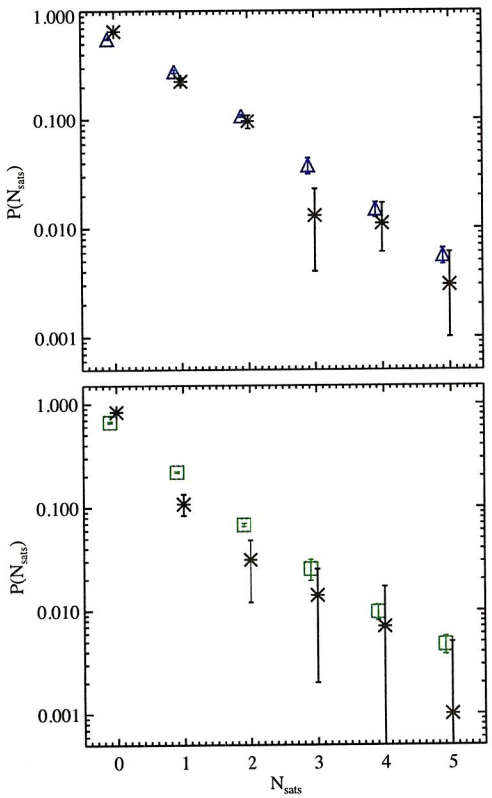

FIG. 8.— *Top Panel:* Abundances of LMC- and SMC-like galaxies around MW-like hosts in SDSS and the Bolshoi simulation. Black stars represent the abundances from SDSS as measured by Liu et al. (2010) using their random background subtraction. The yellow triangles denote the abundance of objects inside a fi xed aperture with radius 150 kpc and length 5.2 Mpc. *Lower Panel:* Same as the upper panel, but now comparing data from Liu et al. (2010) that uses their aperture background subtraction (black stars) as compared to subhalos within 150 kpc from their host center (green squares).

the results from the virial radius by ~~matching~~ to the simulation results. From here, we can recover the tightest agreement for an aperture size of 100 kpc, appreciably lower than the median r_{vir} = 228 for out sample of Milky Way-like hosts. This is roughly the radius where a cylinder centered on an NFW profile with concentration 10 contains the same amount of a mass as is within the virial radius for such a halo, so it should not be surprising that this search radius gives the most consistent result.

One of the appeals of the SHAM algorithm is that it has so few free parameters, in this particular case just the scatter (although there are additional implicit assumptions, e.g. About sub halo stripping). Figure 10 shows how the scatter impacts this result. Here, we present the probability distribution for an isolated host with M_r = –21.2 to host N_{subs} satellites brighter than –16.5 as we vary the scatter in the SHAM model from 0 to 0.3. While none of these models are ruled out by the data, a number of systematic trends are present. In particular, there is a systematic increase in the probability of hosting 3 or more satellites (surprisingly, the probability of hosting two such objects remains virtually unchanged). This trend is caused not by scatter in the mass–luminosity relation of the satellite galaxies, but by the mass–luminosity relation of the host objects. As scatter increases, higher and higher mass hosts scatter into our magnitude-selected sample, bring-

galaxy three point statistics (Marín et al. 2008). Klypin et al. (2010) have shown that a similar procedure can simultaneously match the luminosity function and Tully-Fisher relation locally.

Here, we match halos directly to the binned luminosity function in the local Universe as measured by Blanton et al. (2005) for galaxies with $M_r > -12.8$. While there is some uncertainty in these measurements depending on the detailed surface brightness correction, the objects we are interested in here are bright enough that this effect is unimportant. This luminosity function also reproduces the more recent number densities measured in SDSS DR7 The SDSS Collaboration et al. (2010) down to $M_r \sim -17$. The resulting simulated catalog has a distribution of galaxies that is complete down to $M_r = -15.3$.

Using luminosities assigned in this way, we now make the measurements analogous to those of Liu et al. (2010). We select for Milky Way candidates in the same way as Liu et al. (2010). First, we make a mock lightcone by taking the $z = 0$ SHAM catalog of the Bolshoi simulation, placing an observer at the center of the box, and adding redshift space distortions. We passively evolve galaxy magnitudes to the appropriate redshift using the SDSS constraint $M_r(z) = M_r(z = 0.1) + Q(0.1 - 1)$, with $Q = -1.3$ (Blanton et al. 2003). We then identify all isolated objects by selecting halos with $M_r = -21.2 \pm 0.2$ and excluding objects having a brighter neighbor in a cylinder of radius 500 kpc and length 1000 km s^{-1}. The resulting $v_{\rm max}$ distribution is shown in Figure 5. This distribution is somewhat lower than the best current estimates for $v_{max} = 220$km s^{-1} for the Milky Way (Xue et al. 2008; Gnedin et al. 2010). This should not be terribly surprising; Trujillo-Gomez et al. (2010) have shown that, because the Milky Way sits near the peak of the star formation efficiency, baryons play a significant role in determining the circular velocity profile of Milky Way mass halos, resulting in a value of $v_{\rm max}$ that is underestimated in dark matter only simulations. The virial mass, however, is peaked at $1.3 \times 10^{12} M_\odot$, in excellent agreement with the estimated MW mass from Busha et al. (2010). The Magellanic cloud analogs have $v_{\rm max}$ values of ~ 80 and ~ 70 km s^{-1}, in agreement with the 1-σ constraints from observations(van der Marel et al. 2002; Stanimirović et al. 2004; Harris & Zaritsky 2006).

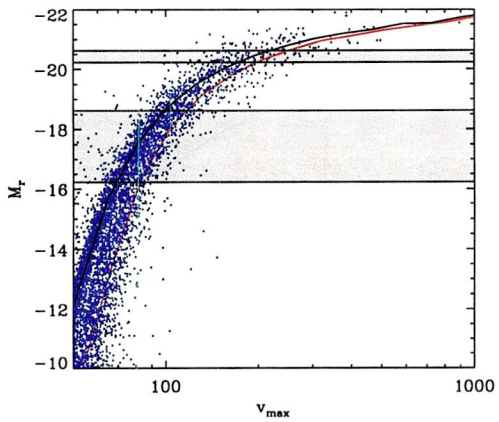

FIG. 4.— The relation between magnitude and v_{max} for our simulated halos+SHAM. The red line represents the relation between M_r and v_{acc}, the maximum circular velocity at the time of accretion, which was used to select the magnitude. The black curve and blue points show the distribution between magnitude and maximum circular velocity at $z = 0$. The upper grey band shows our magnitude-criteria for selecting Milky Way-like hosts, while the lower gray line represents our range for selecting Magellanic Cloud-like satellites.

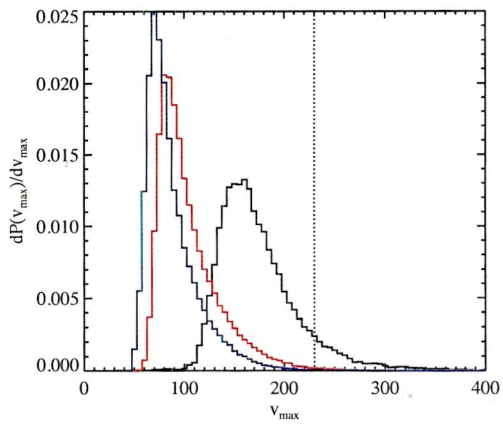

FIG. 5.— The distribution of v_{max} for simulated galaxies, as selected by luminosity. The black histogram represents galaxies that pass our Milky Way selection, with $M_r = -21.2 \pm 0.2$, while the blue and red histograms represent v_{max} and v_{acc} for our Magellanic Cloud-like subhalos that are 2-4 magnitudes dimmer than their hosts. Dotted line shows the preferred value for $v_{\rm max}$ of the MW.

4.3. *The Definitions of a Satellite*

Before presenting detailed comparions between the Liu et al. (2010) data and our model, we note that the definition of a "satellite" differs slightly between the two analyses. Because they were using the SDSS photometric sample with halos selected on luminosity, the number of satellites was defined as the excess above random of the number of objects with appropriate observed magnitude within a projected 150kpc around an isolated Milky Way-magnitude galaxy. The line-of-sight projections are difficult to model in the simulation because the SDSS catalog relied on the observed magnitude of the galaxies, which includes the impact of redshift dimming when looking for neighbors 2-4 magnitudes dimmer. Because the calculation of accurate absolute magnitudes depends on knowledge of the galaxy SEDs, our SHAM model gives us only absolute magnitudes, which are immune to this effect. This projection effect is amplified by correlated structure, which Liu et al. (2010) accounted for. The Bolshoi simulation, however, gives us an additional handle on this constraint, which we approach in two ways. In addition to just counting the number of objects inside the virial radius, we also consider two different cases: 1) where a satellite is an appropriately-bright object within a 150 kpc 3-Dimensional aperture, and 2) where a satellite is an object inside a cylinder of radius 150kpc and length r_0, where r_0 is the correlation scale for the Milky Way host-satellite analog. Both of these numbers can then be compared directly to the measurements from Liu et al. (2010).

This cross-correlation function between MW-luminous galaxies and objects 2-4 magnitudes dimmer is plotted in figure 6, and is well fit by a power-law,

$$\xi(r) = (r/r_0)^{-\gamma} \quad (6)$$

with $r_0 = 5.3$ Mpc/h and $\gamma = 1.7$, very similar to the measurements for all galaxies of this magnitude inferred from The SDSS Collaboration et al. (2010), who measures $r_0 = 5.98$

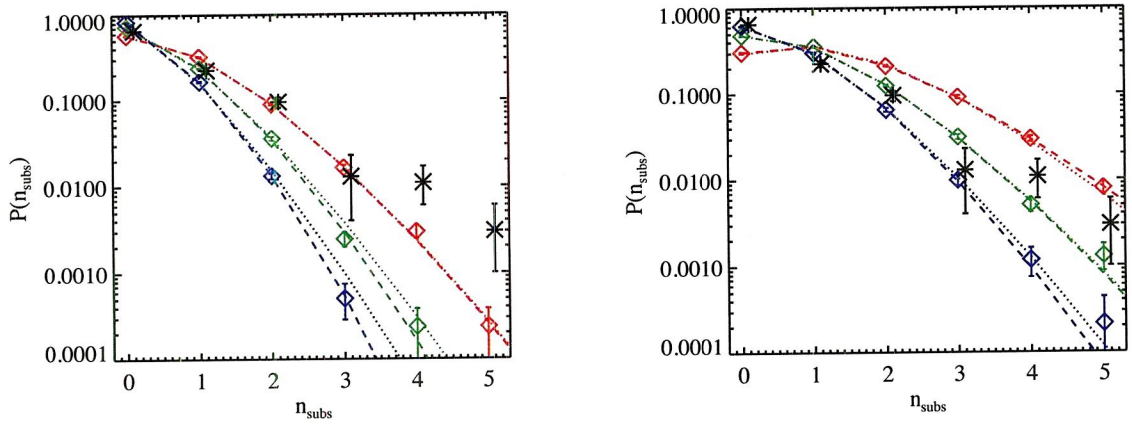

FIG. 1.— Abundance of LMC and SMC-type objects around MW-like hosts in simulations (colored lines) and observations (black points). Left panel shows the results for hosts of mass $M_{\rm vir} \sim 10^{12} h^{-1} {\rm M}_\odot$; right panel considers hosts of mass $M_{\rm vir} \sim 2 \times 10^{12} h^{-1} {\rm M}_\odot$. In both cases, the blue, green, and red distributions correspond to the number of satellites with $v_{\rm max} > 50$, $v_{\rm max} > 60$, and $v_{\rm max} > 70$, respectively. Dashed lines show the best fit negative binomial distribution, and dotted lines show the best fit Poisson distribution. Black points show the observational result of Liu et al. (2010).

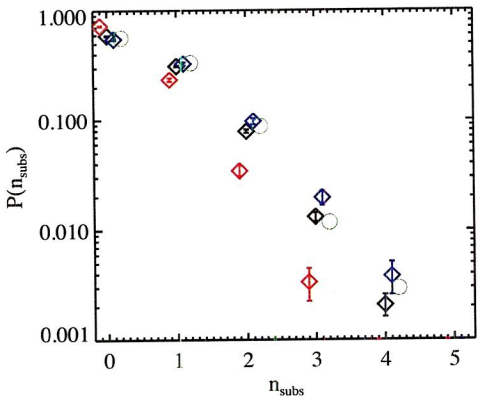

FIG. 2.— The probability that a $1.2 \times 10^{12} {\rm M}_\odot$ halo hosts N_{subs} subhalos with $v_{\rm max} > 50 {\rm km\ s}^{-1}$ split by local host density. The black points represent all halos, while the red and blue points represent the most underdense and overdense quartiles, respectively. Green circles represent MW-mass halos that were selected to have M31-mass neighbors.

3.3. *Probability distributions*

As an extension of the trends shown in in Figure 1, it is useful to generalize these results to arbitrary host and subhalo masses by fitting the probability distribution. A Poisson distribution seems to be the most natural assumption, and has been assumed previously in the literature (i.e., Kravtsov et al. 2004). Deviations from a Poisson distribution can be quantified by the calculation of the second moment, α_2, where

$$\alpha_2 = \frac{\langle N(N-1) \rangle}{\langle N \rangle^2} \tag{3}$$

For a Poisson distribution, $\alpha_2 = 1$. While studies have found some evidence for a deviation from Poisson, with $\alpha_2 > 1$ (Kravtsov et al. 2004; Wetzel & White 2010), the distribution more fully quantified by Boylan-Kolchin et al. (2010). This work found that the distribution could be much better modeled using a negative binomial distribution,

$$P(N|r,p) = \frac{\Gamma(N+r)}{\Gamma(r)\Gamma(N+1)} p^r (1-p)^N \tag{4}$$

where

$$p = \frac{1}{1+(\alpha_2^2-1)\langle N \rangle}, \quad r = \frac{1}{\alpha_2^2-1}, \tag{5}$$

although they note that a Poisson distribution is a reasonable fit when $\langle N \rangle$ is low, such as the case of the MCs. We plot fits to both a Poisson and a negative binomial distribution to our measurements as the dotted and dashed lines in Figure 1. We again see that the, because $\langle N \rangle < 1$, the Poisson distribution provides a reasonable fit, while the negative binomial distribution fit is excellent (at the expense of adding an additional parameter). Note that, when calculating these fits, it is possible to either calculate $\langle N \rangle$ and α directly from the data, or to treat them as free parameters to the fitting algorithm. However, in practice the differences in resulting parameters are less than 5%. While not shown, our results confirm those of Boylan-Kolchin et al. (2010), in that the distribution becomes significantly more non-Poisson for larger values of $\langle N \rangle$.

As a final comparison of the Bolshoi halos to previous work in the literature, we plot in Figure 3 the trends of $\langle N \rangle$ (top panel, similar information to Figure 15 in Klypin et al. 2010) and α_2 (bottom panel) with mass ration $v_{acc,sub}/v_{max,host}$ for a range of host masses. Here, $v_{sub,acc}$ is the maximum circular velocity, v_{max}, that the subhalo had when it was accreted onto its host. As seen in the top panel, the value for $\langle N \rangle$ scales almost self-similarly, but with a slight increase in overall normalization as has been previously noted in the literature (Gao et al. 2004; Klypin et al. 2010; Gao et al. 2010), indicating that more massive halos contain somewhat more substructures, proportionally, than lower mass objects.

More interesting is the trend in α_2 with mass, shown in the lower panel of Figure 3. Here we see evidence that, for subhalos with $v_{max,sub}/v_{max,host} \gtrsim 0.25$, self similarity breaks down much more significantly, where lower mass hosts tend to have systematically higher values of α_2, which correlates with a larger scatter. There are a number of possible explanations for this trend, and it is likely due to the fact that lower mass objects exist in a wider range of environments than higher mass halos. As shown earlier in Figure 2, the immediate environment surrounding a halo can have a significant impact on its subhalo population. High mass halos always form in regions of high bias, meaning that the environmental impact on a high mass objects subhalo population is minimized. Low

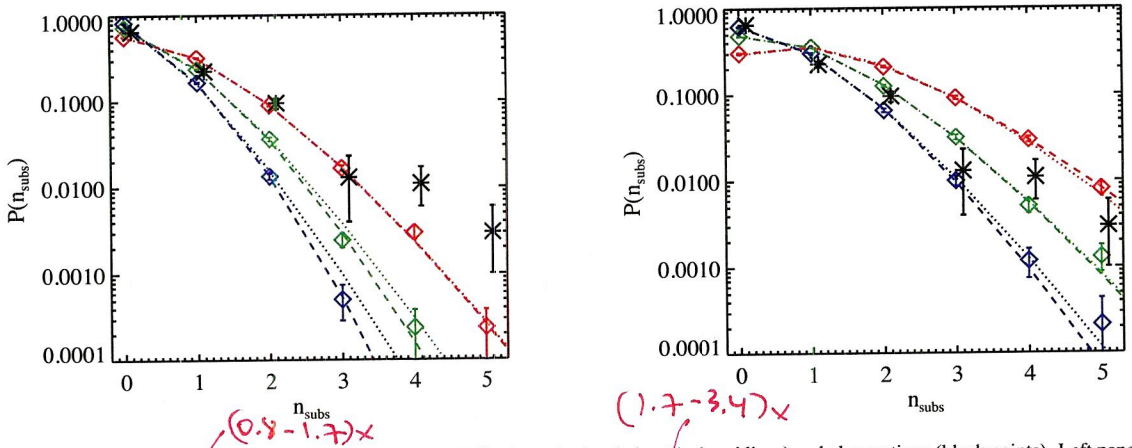

FIG. 1.— Abundance of LMC and SMC-type objects around MW-like hosts in simulations (colored lines) and observations (black points). Left panel shows the results for hosts of mass $M_{vir} \approx 1\times10^{12}h^{-1}\mathrm{M}_\odot$; right panel considers hosts of mass $M_{vir} \approx 2\times10^{12}h^{-1}\mathrm{M}_\odot$. In both cases, the blue, green, and red distributions correspond to the number of satellites with $v_{max} > 50$, $v_{max} > 60$, and $v_{max} > 70$, respectively. Dashed lines show the best fit negative binomial distribution, and dotted lines show the best fit Poisson distribution. Black points show the observational result of Liu et al. (2010).

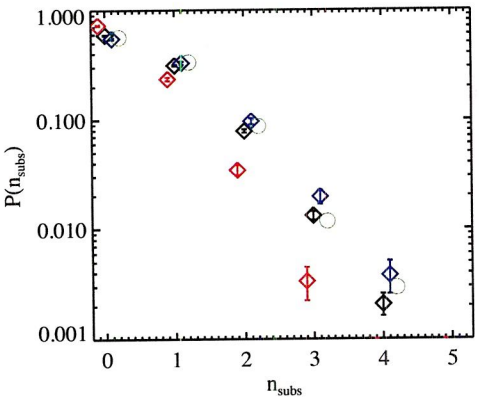

FIG. 2.— The probability that a $1.2\times10^{12}\mathrm{M}_\odot$ halo hosts N_{subs} subhalos with $v_{max} > 50\mathrm{km\ s}^{-1}$split by local host density. The black points represent all halos, while the red and blue points represent the most underdense and overdense quartiles, respectively. Green circles represent MW-mass halos that were selected to have M31-mass neighbors.

3.3. *Probability distributions*

As an extension of the trends show in in Figure 1, it is useful to generalize these results to arbitrary host and subhalo masses by fitting the probability distribution. A Poisson distribution seems to be the most natural assumption, and has been assumed previously in the literature (i.e., Kravtsov et al. 2004). Deviations from a Poisson distribution can be quantified by the calculation of the second moment, α_2, where

$$\alpha_2 = \frac{\langle N(N-1)\rangle}{\langle N\rangle^2} \tag{3}$$

For a Poisson distribution, $\alpha_2 = 1$. While studies have found some evidence for a deviation from Poisson, with $\alpha_2 > 1$ (Kravtsov et al. 2004; Wetzel & White 2010), the distribution more fully quantified by Boylan-Kolchin et al. (2010). This work found that the distribution could be much better modeled using a negative binomial distribution,

$$P(N|r,p) = \frac{\Gamma(N+r)}{\Gamma(r)\Gamma(N+1)}p^r(1-p)^N \tag{4}$$

where

$$p = \frac{1}{1+(\alpha_2^2-1)\langle N\rangle}, \quad r = \frac{1}{\alpha_2^2-1}, \tag{5}$$

although they note that a Poisson distribution is a reasonable fit when $\langle N\rangle$ is low, such as the case of the MCs. We plot fits to both a Poisson and a negative binomial distribution to our measurements as the dotted and dashed lines in Figure 1. We again see that the, because $\langle N\rangle < 1$, the Poisson distribution provides a reasonable fit, while the negative binomial distribution fit is excellent (at the expense of adding an additional parameter). Note that, when calculating these fits, it is possible to either calculate $\langle N\rangle$ and α directly from the data, or to treat them as free parameters to the fitting algorithm. However, in practice the differences in resulting parameters are less than 5%. While not shown, our results confirm those of Boylan-Kolchin et al. (2010), in that the distribution becomes significantly more non-Poisson for larger values of $\langle N\rangle$.

As a final comparison of the Bolshoi halos to previous work in the literature, we plot in Figure 3 the trends of $\langle N\rangle$ (top panel, similar information to Figure 15 in Klypin et al. 2010) and α_2 (bottom panel) with mass ration $v_{acc,sub}/v_{max,host}$ for a range of host masses. Here, $v_{sub,acc}$ is the maximum circular velocity, v_{max}, that the subhalo had when it was accreted onto its host . As seen in the top panel, the value for $\langle N\rangle$ scales almost self-similarly, but with a slight increase in overall normalization as has been previously noted in the literature (Gao et al. 2004; Klypin et al. 2010; Gao et al. 2010) , indicating that more massive halos contain somewhat more substructures, proportionally, than lower mass objects.

More interesting is the trend in α_2 with mass, shown in the lower panel of Figure 3. Here we see evidence that, for subhalos with $v_{max,sub}/v_{max,host} \gtrsim 0.25$, self similarity breaks down much more significantly, where lower mass hosts tend to have systematically higher values of α_2, which correlates with a larger scatter. There are a number of possible explanations for this trend, and it is likely due to the fact that lower mass objects exist in a wider range of environments than higher mass halos. As shown earlier in Figure 2, the immediate environment surrounding a halo can have a significant impact on its subhalo population. High mass halos always form in regions of high bias, meaning that the environmental impact

models to add galaxies to some of the high resolution Aquarius halos (Springel et al. 2008). It was again difficult to readily reproduce halos with MC-like luminosities. Having looked in detail at a handful of simulated objects, however, this work indicates that there may be significant halo-to-halo scatter as to the presence of such massive objects. The idea of intrinsic scatter in the halo relation was expanded on in Ishiyama et al. (2009a). While this work did not concentrate specifically on MC-like subhalos, they did consider the range in number of subhalo $v_{max,sub}/v_{max,host} > 0.1$. This work showed an extremely large variation (20-60) in the number of massive subhalos a galaxy-sized halos would host.

In contrast to the above work, Libeskind et al. (2007) used hydrodynamic simulations to model the luminosity functions for the satellites around Milky Way-like host halos. Their simulation identified 9 Milky Way-like central galaxies and found that they, on average, have 1.6 satellites brighter than $M_V = -16$ and a third of them had satellites with luminosities comparable to the LMC.

The recent Bolshoi and Millennium-II simulations (Klypin et al. 2010; Springel et al. 2008) have, for the first time, allowed us to probe cosmological volumes to understand the ΛCDM predictions for the satellite populations of Milky Way like halos. Such measurements were recently made by Boylan-Kolchin et al. (2010) who quantified the likelihood for $10^{12}\mathrm{M}_\odot$ halos to host massive satellite galaxies in the Millennium-II simulation. In this paper, we expand on this work by making similar measurements for the Bolshoi simulation, and using an abundance matching technique to assign luminosities to halos and make detailed comparisons between the Bolshoi predictions and the measurements from Liu et al. (2010). Our goal is to understand just how well ΛCDM reproduces the statistical properties of lower mass galaxies.

Note that this is the reverse question that was asked in a companion paper, Busha et al. (2010). That work assumed a satellite population and asked what implications were made for the mass of the host halo. Here, we assume a host halo mass and ask about the implications for the subhalo population. There is no reason for both questions to give the same answer. For example, while Busha et al. (2010) showed that a $1.2 \times 10^{12}\mathrm{M}_\odot$ halos was the most likely object to host two MC-like satellites, there is no reason to assume that a typical $1.2 \times 10^{12}\mathrm{M}_\odot$ halo will have the MCs as satellites.

We begin by giving an overview of the Bolshoi simulation used in §2, before proceeding to §3 to investigate the properties of massive dark matter satellites around dark matter host halos, focusing on the mass range for hosts and satellites that is relevant to the MW system. The analysis here is similar to that of Boylan-Kolchin et al. (2010). In §4, we assign galaxy luminosities to our suite of dark matter halos and extend the results for a sample that is selected similar to the observations. Using this algorithm we are able to make detailed comparisons to the work of Liu et al. (2010) concerning the satellite population around Milky Way magnitude galaxies. Finally, in §5, we expand this study to include the satellite population of a more general distribution of hosts. Throughout this paper, we adopt the convention $h = 0.7$ when reporting values from either simulations or observations.

2. SIMULATIONS

We use the dark matter halos identified in the Bolshoi simulation (Klypin et al. 2010; Trujillo-Gomez et al. 2010). This simulation modeled a 250 h^{-1}Mpc comoving box using cosmological parameters similar to those derived by WMAP7 (Komatsu et al. 2010): $\Omega_m = 0.27$, $\Omega_\Lambda = 0.73$, $\sigma_8 = 0.82$, $n = 0.95$, and $h = 0.7$. The simulation volume contains 2048^3 particles, each with a mass of $1.15 \times 10^8 h^{-1}\mathrm{M}_\odot$ and was run using the ART code (Kravtsov et al. 1997). 180 snapshots from the simulation were saved and analyzed. One of the unique aspects of this simulation is the high level of spatial resolution employed, allowing objects to be resolved down to a physical scale of 1 h^{-1}kpc. This gives us excellent ability to track halos as they merge with and are disrupted by larger objects, allowing us to track them even as they pass near the core of the halo.

Halos and subhalos were identified using the BDM algorithm (Klypin & Holtzman (1997). The algorithm identifies maxima in the density field examines the neighboring region to identify bound particles. In this way, it treats both halos and subhalos identically, and subhalos are just identified as objects living within the virial radius of a larger objects. Because of the high level of mass and spatial resolution, BDM results in a halo catalog that is complete down to a maximum circular velocity $v_{\max} = 50$ km s^{-1}, where

$$v_{\max} = \max\left(\sqrt{\frac{GM(<r)}{r}}\right). \quad (1)$$

This corresponds to a virial mass of roughly $10^{10} h^{-1}\mathrm{M}_\odot$. When BDM halos are identified, the id's of their 50 most bound particles are also stored to assist in producing merger trees.

As discussed in Section 4.2, in order to assign galaxy luminosities to dark matter halos, we need to track the histories of dark matter substructures. This is done using merger trees created from 180 snapshots of the Bolshoi simulation. The detailed algorithm for creating the merger trees is described in Behroozi et al. (2010a). Briefly, the algorithm works by first linking halos across time-steps by tracking the 50 most bound particles of each halo. Clearly, some halos will not have any of their 50 most bound particles identified at a later time steps (ie.: very massive objects where the 50 most bound particles will change rapidly through stochastic processes), while some will have their particles distributed to multiple halos. The algorithm corrects for this by running a simple N-body calculation on the locations and masses of all halos in simulation to get a prediction of where each halo should wind up at the next time step. Using this information, it is possible to link halos across multiple time steps to very high accuracy.

3. SATELLITE STATISTICS FOR DARK MATTER SUBHALOS

We begin by investigating the properties of dark matter satellites around dark matter hosts in the Bolshoi simulation, focusing on the mass range for hosts and satellites that is relevant to the MW system. In §3.1, we consider trends with host halo mass, in §3.2 we investigate trends with halo environment. We then consider the distribution of the satellite number §3.3. In the subsequent section, §4, we extend this analysis to include a more observationally-relevant selection on galaxy luminosities.

Because the mass resolution of the Bolshoi simulation creates a halo catalog complete down to 50 km s^{-1}, roughly equivalent to the lower bound of the mass of the SMC, we begin by measuring the likelihood of hosting N_{subs} subhalos more massive than a given $v_{\max}$. This measurement is made by identifying the virial radius of all distinct (non-subhalo)